 doi:10.20944/preprints201807.0464.v1

Article Paper

Corrosion Susceptibility of Surface Etched Ultrafine Grained Titanium and its Alloys under Physiological Environment

Daniel Fernandes[1,2,*], Egor Prokofiev[3], Ruslan Valiev[3,4], Ana Almeida[1], Emilia Monteiro[1] and Carlos Elias[1]

[1]Biomaterials Laboratory, Instituto Militar de Engenharia, Rio de Janeiro, RJ 22290-270, Brazil.
[2]School of Engineering, University of South Australia, Mawson Lakes, SA 5095, Australia.
[3]Saint Petersburg State University, St. Petersburg 199034, Russia.
[4]Institute of Physics of Advanced Materials, Ufa State Aviation Technical University, Ufa 450000, Russia
*Correspondence: djfernandes@ime.eb.br; Tel.: +55-21-2546-7080 (ext. 6848)

Abstract: 1)Background: The objective was to evaluate the corrosion resistance of different commercially pure ultrafine-grained (UFG) titanium and its alloys with acid etched surface processed by equal-channel angular pressing (ECAP); 2) Methods: Coarse-grained and UFG titanium samples were investigated using polarization resistance technique. Surface characteristics of the native oxidized layer were evaluated by TEM and XRD. Electrochemical tests were under physiological electrolyte at a rate of 1 and 10 mV/s. Weight loss tests were performed after immersion into HCl solution for up to 3 years; 3) Results: UFG titanium was less susceptible to corrosion which was identified under lower rates and at higher polarization resistance than its coarse grain counterparts. Titanium Grade 2 and Grade 4 demonstrated similar corrosion susceptibility. Titanium Grade 5 revealed a thin and tightly adhered native oxide layer with adequate corrosion resistance; 4) Conclusions: ECAP process imposed a more compact and adhered oxidized layer. Surface etching techniques delivered a thicker native TiO_2 layer, being both grain refinement and surface etching techniques responsible for the improved corrosion resistance of Titanium samples under physiological environment after 3 years of observation. **Keywords:** corrosion 1; plastic deformation 2; titanium 3; titanium alloys 4; surface treatment 5.

1. Introduction

The outstanding corrosion resistance of titanium, as well as its adequate biocompatibility, made it one of the most widely used biomaterial for biomedical osseointegrated implants [1]. Beyond that, other highlighted properties include Young's modulus closer that of the bone, low density, good ductility, and a positive effect on skeletal cell agents imposed by the microenvironment provided by titanium oxide layer. Surfaced oxide layer is also responsible for improvements in corrosion resistance and thus in the reduction of metallic ions release [2,3].

The main concern of titanium under biomedical service is its high friction coefficient and severe abrasive wear, with great susceptibility to fretting wear and substantial amounts of titanium debris production [4]. The metallic debris release comes from the fracture and surface abrasion, which is able to break down the passive layer, leading to metallic deposition in local tissue and toxic ions release. This potential toxicity may conduct to neurological pathologies, particle induced inflammation and hypersensitivity in human body, and therefore it should be avoided [2].

With the purpose to prevent ions release using of commercially pure (CP) titanium are preferred instead of titanium alloys. Although titanium ASTM Grade 5 (G5) has excellent mechanical strength due to the presence of alloying elements like Al and V, these elements are designed as toxic. Their release is currently expected as a consequence of corrosion degradation and is considered hazardous due to cumulative effects into biological environments [5]. In that framework, different processing

 doi:10.20944/preprints201807.0464.v1

techniques have been developed to improve the mechanical performance of CP titanium ASTM Grade 4 (G4), which are absented of the toxic alloying elements. Development of severe plastic deformation (SPD) techniques [6] has made it possible to form ultrafine-grained (UFG) microstructure in CP titanium, which resulted in enhancement of its mechanical strength, fatigue properties and promote improvements into passive oxidized layer features. [5,7-12]. Equal-channel angular pressing (ECAP) and continuous ECAP-Conform (ECAP-C) impose grain refinement for each pass of sample through the die, whereas a higher shear strain state is gradually achieved, i.e. equiaxial grain/subgrain sizes between 150-300 ηm with high-angle boundaries were identified after 4-6 passes [6].

Innumerous experiments have been performed to analyze the corrosion resistance of the Ti-based alloys [13]. Different methods included surface treatments by anodic oxidation, acid immersion or any other procedure that can modify surface energy and its interactions with environment. Surface etching is employed to promote improvements into surface energy, with ability to boost characteristics of surface roughness and its wettability, which are both relevant during attempts to enhance biocompatibility [3,10,12]. Even processing techniques mainly aimed for grain refinement of titanium materials can induce changes in corrosion resistance due to alterations of the characteristics of the passive oxidized layer [3]. The objective of this work was to evaluate the corrosion resistance of distinct types of UFG titanium samples processed by ECAP technique and compare them with its coarse-grained state with and without surface etching treatment.

2. Materials and Methods

Different commercially pure titanium and its alloys in shape of 3 mm in height cylinders were prepared for the study. Table 1 presents sample conditions used for investigation including composition, processing condition, grain size and surface features. The details of ECAP and ECAP-Conform processing and optimal regimes of UFG structure formation have been described in previous studies [6,8].

Three millimeters in height cylinders were metallographically prepared. Etching was performed by HCl and H_2SO_4 solution with the same concentration, temperature and time interval. Specimens were ultrasonically cleaned in acetone and dried at room temperature. An additional sample of each group with 100 μm in thickness was prepared for TEM analysis under electropolishing preparation in an electropolisher TenuPol-5 (Struers, Denmark) with perchloric acid, ethanol and butanol solution under a current of 1A. The process was electronically halted when the smallest possible hole was achieved. Surface etched specimens could not be analyzed by TEM since electropolishing preparation interferes into characteristics of the morphology and topography of its surfaces.

Phases identification of the passive oxidized layer was performed by an X-ray diffractometer X´Pert 2 (Panalytical, Netherlands) with a Cu-Kα (λ= 1.5405 Å) at 40 KV and 40 mA at grazing incidence set up at θ=0.5°, in the 2θ range 20-70° with a step size of 0.05°.

Electrochemical analysis was performed by a potentiostat instrument (PGSTAT302N, Autolab) using a three-electrode flat cell with saturated calomel electrodes as reference and platinum as counter one. Samples were inlayed in Teflon with a standardized exposed surface of 1 mm^2, at a distance of 1 cm from the reference electrode and 10 cm from the counter electrode. Specimens were immersed into a cell filled with 100 mL of physiological solution (pH=7.4) of NaCl (0.9 mol L^{-1}) as electrolyte at 37°C for 2 hours. Polarization curves were acquired under an open circuit potential at a scan rate of 1 and 10 mVs^{-1} for all specimens evaluated and merged for further comparison and calculations.

Weight loss analysis was performed at cylinder shape specimens with diameter of 6 mm and 4 mm in height, which were weighted before and after immersion into 1M HCl solution for 1440 hours (2 months). Samples were reweighted 3 years after the first measurement.

3. Results

The corrosion potential identified in figure 1 revealed that UFG-C samples have the lowest potential followed by G5>G5-P>G4>G2>UFG and UFG-C-P. Grain sizes ranged from average regular

Preprints (www.preprints.org) | NOT PEER-REVIEWED | Posted: 25 July 2018 doi:10.20944/preprints201807.0464.v1

size 25 μm (G4) to 0.3-0.15 μm after refinement (table 1). Open circuit potential (table 2) was read as -0.174V from G2, -0.166V from UFG-C-P, -0.152V from G4, -0.151V from UFG, -0.128V from G5, -0.110V from G5-P and -0.098V from UFG-C. Tafel intersections, based on polarization curves, βc= -0.042 $Vdec^{-1}A^{-1}cm^{-2}$ and βa= 0.025 $Vdec^{-1}A^{-1}cm^{-2}$ from G2 samples. Gradients from G4 specimens showed βc= -0.034 $Vdec^{-1}A^{-1}cm^{-2}$ and βa= 0.027 $Vdec^{-1}A^{-1}cm^{-2}$ and reflect similar slopes in cathodic curve. Both curves reached corrosion potential at similar current density and corrosion potential (Table 2), although G4 samples reached equilibrium between oxidation and reduction at higher potential (-0.399V vs -0.421 V), being the slope of anodic curve greater in G4 samples. Critical current density was higher recorded at G4 and G4h samples, polarization resistance was larger at G5-P and IFG-C, and corrosion rate was lowest at UFG-C and highest at G2 samples. TEM identified oxide layers with qualitative variances in organization (figure 2), at different thickness from samples as UFG (51.045 ηm), G2 (12.102ηm), UFG-C (10.515 ηm) and G4 (5.17 ηm). Diffractograms (figure 3) at grazing incidence exposed mainly the anatase variant of titanium oxide layer. Weight loss (figure 4) demonstrated minor differences among samples with the lowest loss from UFG and UFG-C-P and largest from G2 samples after 2 months. After 3 years, all samples revealed weight increase, except G5 samples where a loss of 0.98% was identified.

3.1. Figures, Tables and Schemes

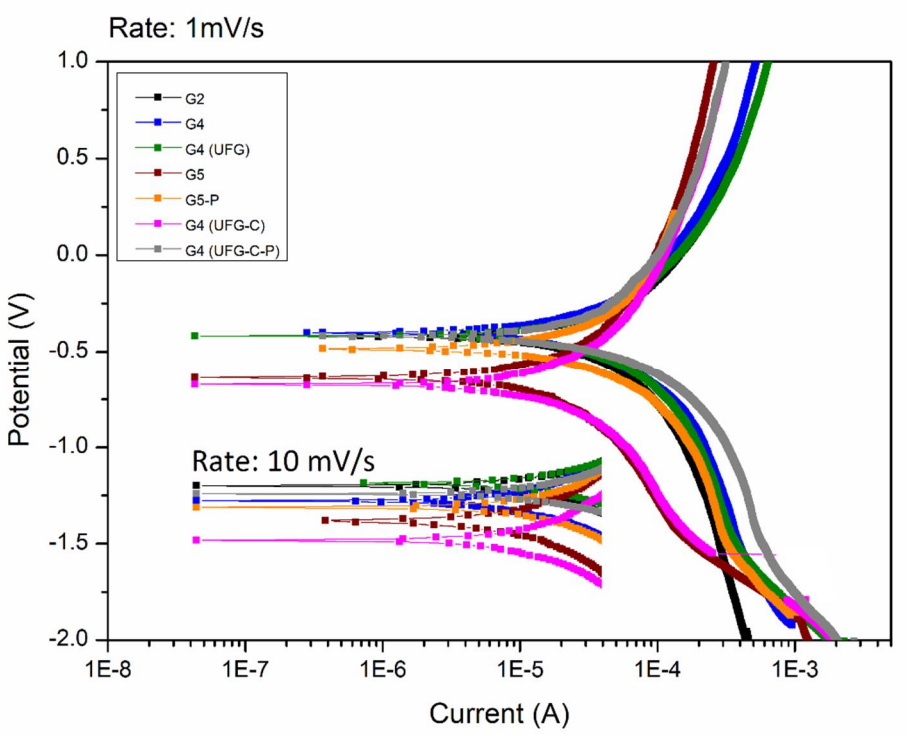

Figure 1. Polarization curves from different titanium samples.

Preprints (www.preprints.org) | NOT PEER-REVIEWED | Posted: 25 July 2018 doi:10.20944/preprints201807.0464.v1

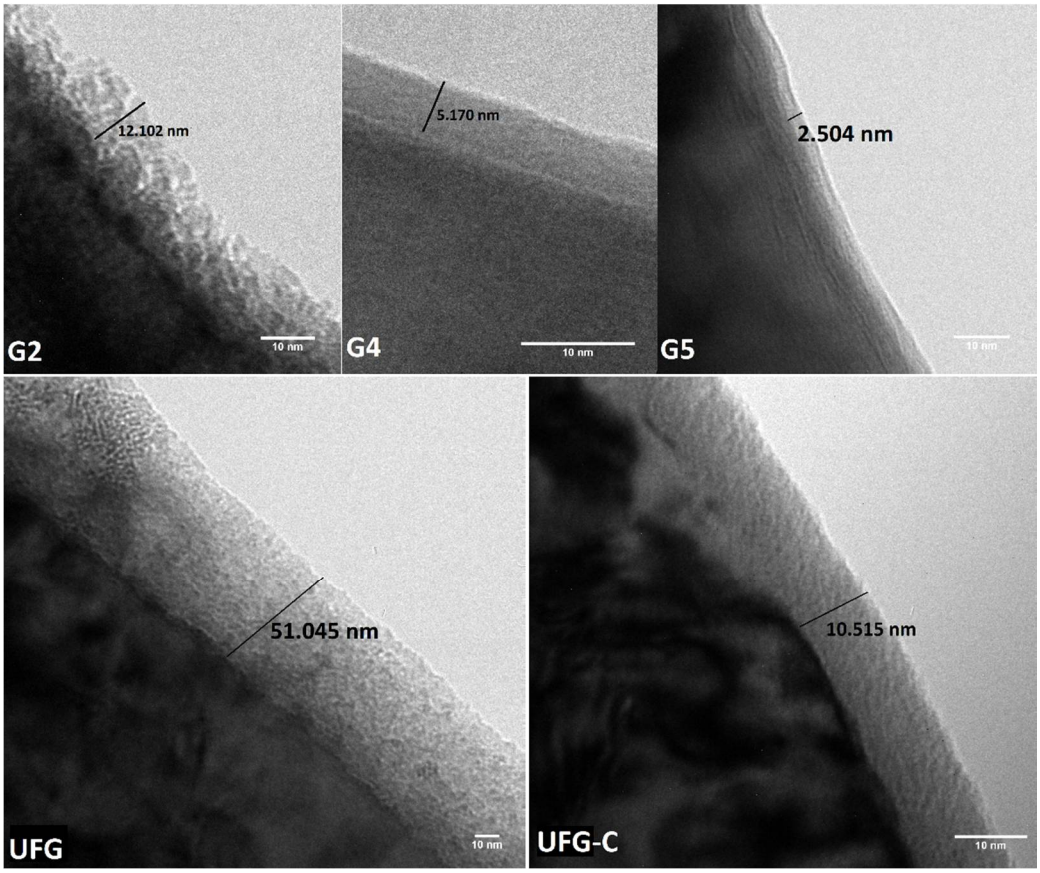

Figure 2. TEM micrographs revealed the morphology of the native oxide layer. The thickness of the film is indicated.

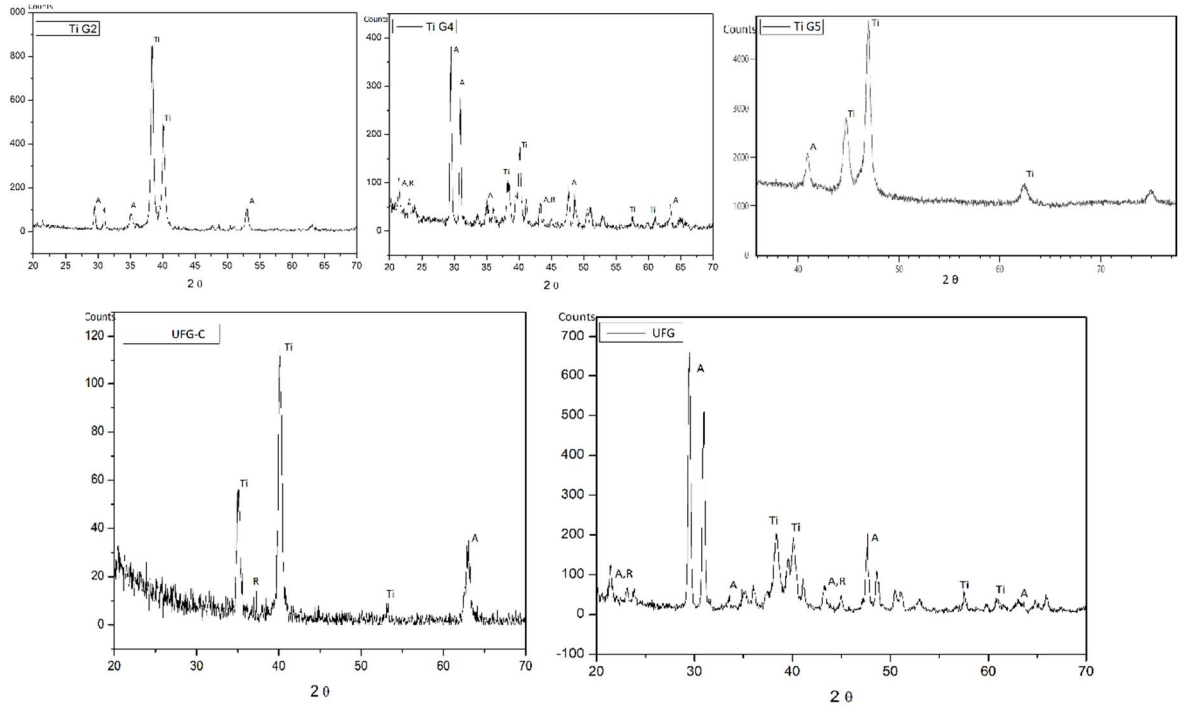

Figure 3. Diffractograms at grazing incidence of the native oxide layers showed at figure 2.

Preprints (www.preprints.org) | NOT PEER-REVIEWED | Posted: 25 July 2018 doi:10.20944/preprints201807.0464.v1

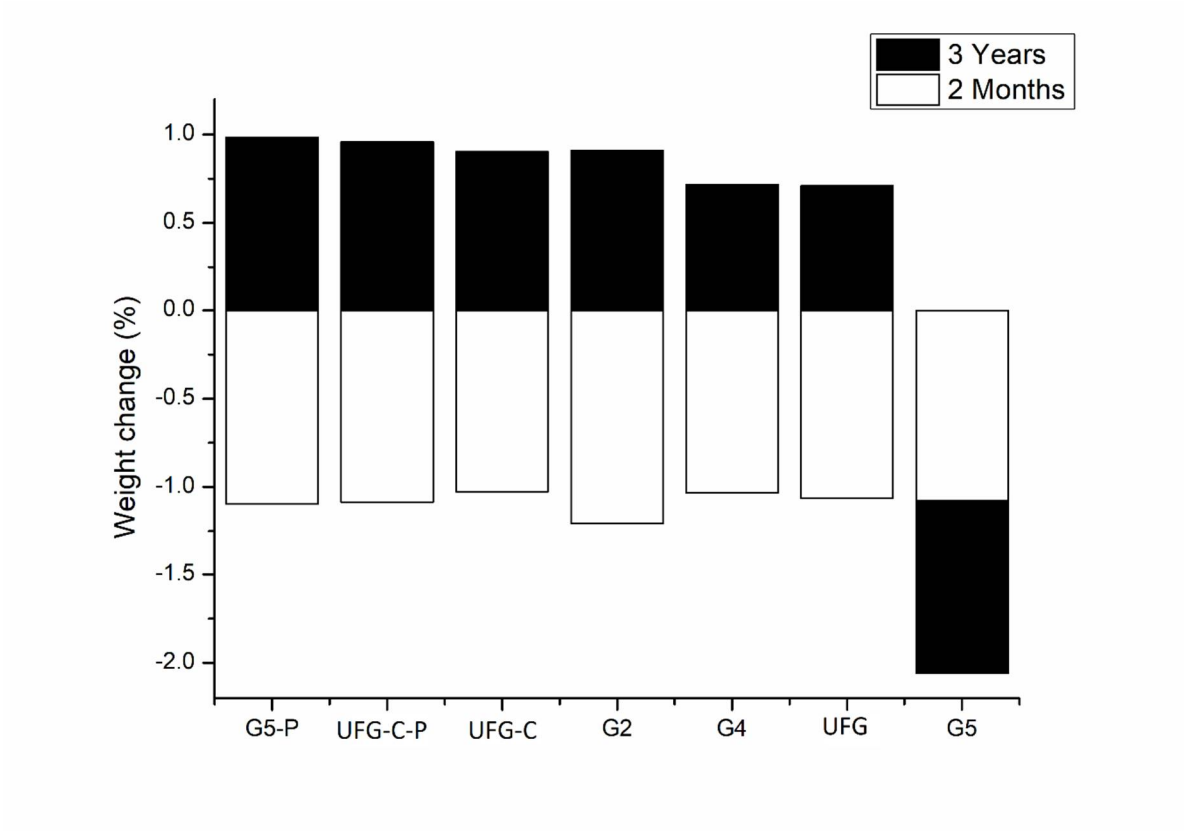

Figure 4. Weight loss test after 2 months and an additional follow up of 3 years. Samples were immersed into 1M HCl solution. Values are given in (%) and positive values indicated weight gain.

Table 1. Sample condition of titanium its alloys used for investigation.

Sample condition	ASTM Grade	Processing condition	Average grain size (μm)	Surface treatment
G2	Grade 2	As-received	-	-
G4	Grade 4	As-received	25	-
G5	Grade 5	As-received	-	-
G5-P	Grade 5	As-received	-	Acid etched
UFG	Grade 4	ECAP	0.3	-
UFG-C	Grade 4	ECAP-Conform +drawing	0.15	-
UFG-C-P	Grade 4	ECAP-Conform +drawing	0.15	Acid etched

Preprints (www.preprints.org) | NOT PEER-REVIEWED | Posted: 25 July 2018 doi:10.20944/preprints201807.0464.v1

Table 2 – Open circuit potential (OCP), corrosion current density (Icorr), corrosion potential (E_{Corr}), Tafel coefficients (β_a and β_c), primary passive potential (E_{pp}), critical current density (I_c), polarization resistance and corrosion rate from different samples. Rate was settled at 1 mV/s.

Samples	OCP (V)	Icorr (A/cm²)	E_{Corr} (V)	β_a	β_c	E_{pp}	I_c	Polarization Resistance (ohm/cm²)	Corrosion rate (10^{-3} mm/year)
G2	-0,174	4,69E-05	-0,421	0,025	-0,042	0.568	3.905E-4	145,579	0,807
G4	-0,152	4,82E-05	-0,399	0,027	-0,034	0.979	5.311E-4	136,748	0,829
G4h	-0,151	4,47E-05	-0,421	0,026	-0,032	0.972	6.367E-4	139,248	0,769
G4(UFG)	-0,098	2,01E-05	-0,674	0,034	-0,016	0.892	3.019E-4	235,374	0,347
G4(UFG-P)	-0,166	4,07E-05	-0,421	0,036	-0,022	0.976	3.167E-4	143,908	0,701
G5	-0,128	2,20E-05	-0,638	0,039	-0,019	-0.016	9.729E-5	251,397	0,379
G5-P	-0,11	2,76E-05	-0,485	0,021	-0,024	0.212	1.358E-4	175,360	0,475

4. Discussion

Different behavior was observed in the superimposed polarization curves showed in Figure 1. Although the corrosion potential brings limited information regarding corrosion rates, results revealed that UFG-C samples has the lowest potential followed by G5, G5-P, G4, G2, UFG and UFG-C-P.

Open circuit potential (Table 2) was read as -0.174V from G2, -0.166V from UFG-C-P, -0.152V from G4, -0.151V from UFG, -0.128V from G5, -0.110V from G5-P and -0.098V from UFG-C. Comparison among the several open potentials revealed that the most chemically stable values were acquired from UFG, however the samples became significantly instable (-0.166V) after etching surface treatment. The OCP value from UFG-C-P was the lowest measured, except for the value from G2 (-0.174V). This behavior was not observed in titanium alloys, where potential was increased after acid etching surface treatment, becoming the etched G5 titanium chemically more stable (-0.128V) than samples before surface etching (-0,110V). Regarding the stability of coarse-grained CP Ti samples, G4 specimens showed higher OCP value (-0,152V) than G2 (-0.174V), which could be explained in terms of the higher continuous tightly adherent oxide layer expected (Figure 2), besides higher levels of oxygen, nitrogen and iron are also expected. Although UFG specimens showed the thicker native film (Figure 2), its corrosion behavior was less affected by changes in microstructure than observed in UFG-C specimens, since OCP values were similar (difference of just 0.001V) when compared to its coarse-grained state.

Tafel intersections were defined basing on polarization curves. Tafel constants were βc= -0.042 $Vdec^{-1}A^{-1}cm^{-2}$ and βa= 0.025 $Vdec^{-1}A^{-1}cm^{-2}$ from G2 samples. Gradients from G4 specimens showed βc= -0.034 $Vdec^{-1}A^{-1}cm^{-2}$ and βa= 0.027 $Vdec^{-1}A^{-1}cm^{-2}$ and reflect similar slopes in cathodic curve. Both curves reached corrosion potential at similar current density and corrosion potential (Table 2), although G4 samples reached equilibrium between oxidation and reduction at higher potential (-0.399V vs -0.421 V), being the slope of anodic curve greater in G4 samples.

Comparing cathodic and anodic curves (Figure 1), differences in slopes can be identified and reflect straightly in Tafel constants. Despite the initial overlap of cathodic curves from alloys, they assumed different slopes when potential is raised by potentiostat, being UFG-C cathodic slope lower than the others. However, the tangent related to the UFG samples etched was lower, the specimen took more time to be polarized, which justify the right slide of curve when compared to mainly of the other titanium samples. After passivation oxide film is being formed, UFG-C presented a passivation ability under lower potentials. This reflects in anodic constants, which slope was almost vertical, while an angle of almost 45° with a slope of 1 was identified from at least 3 of the other

 doi:10.20944/preprints201807.0464.v1

samples, with exception of the etched UFG-C and UFG one. Gradients before and after surface etching revealed similar behavior under cathodic and anodic reactions (Table 2), although corrosion potentials were whole slid up after etching. Corrosion current density (I_{corr}) was less affected by surface treatment. Comparing electrochemical behavior of samples submitted to ECAP and its coarse-grained counterparts, UFG-C specimens showed a lower resistance to corrosion than cold-worked UFG samples. UFG demonstrated an upper slide in comparison to coarse-grained G4 curve, while UFG-C curve stayed below G4 curve. In this perspective, UFG samples had a slightly higher corrosion potential (E_{corr}) than G4 and UFG-C.

The influence of changes in substructure and chemical stability of titanium alloys are widely reported [3,14,15]. Although grain boundaries are commonly expected areas susceptible to corrosion attack, the increased chemical stability of UFG might be related to improvements into protective passivation film achieved due to changes in surface energy (Figure 2). Somehow, the influence of microstructure evolution on film stability can be related to the degree of achieved refinement, since UFG-C specimens demonstrated limited ability to increase its corrosion resistance, although the current density was similar and corrosion potential stayed close to observed in UFG specimens. Discussion upon the degree of grain refinement of cold worked samples in comparison with UFG-C is found in [12].

Weight loss analysis was performed as usually shown in literature [14] with a couple months of follow up and an additional observation was performed after a lengthy period of immersion in acid solution. A follow up of 3-year after a regular immersion for 2 months can reveal a precise insight of the dynamic process of corrosion based on its weight change. Figure 4 shows weight alterations after 2 and 38 months. In 2 months all samples demonstrated similar weight loss, varying from 1.02% (UFG-C) to 1.2% (G2). Slight difference was observed between specimens before and after surface etching (0.02%-0.06%), while the difference between work hardening of G4 specimens (UFG-C and UFG) was less than 0.04%.

The primary passive potential (Table 2) determines when passivation is initiated. From our results, oxidized layer was first formed in Ti-6Al-4V samples (G5 and G5-P) and specimens (G4-UFG-C), being the values of potential close to G2 samples. Similar values of potential were recorded from ultrafine-grained (UFG and UFG-C), etched UFG-C-P, and G4 specimens. Although values stayed in a close range, the greater potential was recorded in G4 specimens.

The values of critical current density (Table 2) were smaller in specimens where passivation process was firstly initiated, as seen in Ti-6Al-4V samples (G5 and G5-P). Similar current was measured in ultrafine-grained (UFG and UFG-C) and coarse-grained G2. Higher current densities were recorded in G4h and G4 samples. These results confirm the importance of the oxide layer in corrosion protection of the specimens, since the intensity of current density was lower in samples passivated at lower potentials and higher at samples passivated later at higher potentials. Polarization (Table 2) was also in alignment with the discussed above relation between current and passivation, once the resistance to electrons passage is in opposite relation to the values of current density measured.

Coarse-grained non-etched G4, UFG, UFG-C-P and G2 samples demonstrated lower polarization resistance which have allowed the highest current density passaged, being the specimen passivated at highest potential. Etched Ti-6Al-4V (G5-P) and UFG-C showed higher resistance to polarization, which is, however, lower than that of non-etched Ti-6Al-4V (G5) samples. The highest resistance to current passage from Ti-6Al-4V (G5) was in coherence with the lowest density of measured current (I_c) and the lowest potential of passivation (E_{pp}) described above.

Comparing the values of primary passivation and the density of current with the weight loss presented above (after 2 months), minor differences were observed in the loss among the specimens evaluated. However, differences were below 0.01%, UFG-C specimens demonstrated the lowest weight loss with identical values from observed in UFG and UFG-C-P specimens. The greatest loss was identified in G2 samples, which susceptibility might be related to changes in tightly adherence of oxide layer, as seen in Figure 2, where even before immersion into acid solution G2 samples had already demonstrated a less tightly dense oxide film. On the other hand, the densest film was

 doi:10.20944/preprints201807.0464.v1

observed in UFG-C and G4 specimens, with a thickness of 10.515 ηm and 5.170 ηm, respectively. G5 samples demonstrated the densest and the thinnest (2.504 ηm) oxide film. UFG samples demonstrated the thickest (51.045 ηm) film, however, with a not so tightly dense layer. These findings are in line with our results regarding polarization curves, polarization resistance, corrosion rate and weight loss. At grazing incidence, the native titanium layer was identified as mainly formed by anatase variant (Figure 3).

Corrosion rate extrapolations in mm/year confirmed the projections of the least weight loss of UFG-C and a higher rate of coarse grain G2 samples. Considering the short range of difference among weight loss discussed above, weight loss extrapolations were in accordance with the intermediate values of G5 alloy (G5-P and G5), UFG-C-P, UFG and a higher weight loss of coarse-grained G2. It was interesting to observe that etching surface treatment had slight increased the weight loss after 2 months of immersion into acid solution when comparisons were performed with its counterpart coarse-grained specimens.

The 3-year long-term weight loss followed up and was necessary since extrapolations would not be able to predict the possible weight increase due to the passive layer thickening that comes after oxidation process. After 38 months of immersion in HCl, our results revealed a weight increase in all specimens, except Ti-6Al-4V alloy (G5) which had a decrease of 0.98% (Figure 4). Mass increase was observed at a very close range of 0.7%-0.98%, even between UFG and coarse grain (G4) specimens. Identical mass increase was found in UFG-C, coarse grain G2, UFG-C-P and etched Ti6Al4V (G5-P) samples. Changes in weight loss behavior were identified in acid etched surface treated specimens when follow up was extended from a regular analysis of 2 months to a period of 38 months. In this perspective, etched samples demonstrated the highest increase of mass and reflect improvements in passive film stability and enhancements into corrosion resistance. This finding was not observed after 2 months, what implies that an extended follow up was necessary to diagnose any changes in passivation oxide layer features, including its thickness and/or alterations in its continuous tight adherence. Weight gain is predictable in cases of oxidation process by different laws [16-18], and oxidation reactions are adequate descripted by Cabrera-Mott model and its modifications [19]. Oxidation kinetics can be assumed in terms of inverse logarithm law during film grow [17], although the effectiveness of a conventional thermally activated diffusion model is limited and unable to interpret low temperatures differential data [20]. Oxidation process under low temperature environment can be predicted in terms of weight gain by parabolic and linear laws with one third of the power expected at temperatures of 400-500°C [16]. At 600°C mass gain was also predicted by a linear law [18], being the first power of time, and weight gain considered adequate when small amount of mass has already been deposited as a consequence of oxide film thickening [16]. In terms of Carrera-Mott model, weight gain [17] was compared with our results and the thickness of oxide layer was extrapolated in keeping with aluminum kinetics [20] due to absence of models with titanium under identical thermodynamic conditions. This extrapolation reflected an increase of passive layer in rage of 0.624-0.682 ηm. In consonance with the weight gain presented above, oxide layer thickening of cold worked and coarse grain G4 titanium was identical (0.624 ηm), followed by etched Ti6Al4V (0.643 ηm), UFG-C (0.655 ηm), coarse grain G2 (0.666 ηm) and UFG-C-P (0.682 ηm). Despite thickness increase was similar, etched surfaces demonstrated improved potential of enhance passive layer organization in terms of weight gain and oxide film dimensions.

The positive influence of processing techniques in polarization behavior was observed at samples subjected to ECAP. From ultrafine-grained materials (UFG and UFG-C) standpoint, any improvement in corrosion resistance that might arise from the ultrafine microstructure sounds controversial. Generally, any increase in the grain boundary density would be expected to decrease the corrosion resistance of the material, since boundaries might work as preferable sites for nucleation of pits. On the other hand, our results showed that the corrosion susceptibility was reduced, the higher relative boundary-related material volume improved the weight gain, oxide layer thickness and polarization behavior become ruled by terms of passivation kinetics. Therefore, a faster and stable passive layer was formed by reason of the high relative grain boundary related volume of ultrafine grained samples. This perspective is in accordance with findings reported in [2,14], and was

also identified in Figure 2 where a denser, thicker and a more homogeneous oxide layer was addressed to surface of ultrafine grained samples. Apart from grain boundary influence, dislocations might also be considered during our discussion. Dislocations are identified as high energy linear defects with greater susceptibility for pits nucleation, with an opposite effect from its density inside the grains and the overall corrosion resistance [14]. Confronting ultrafine-grained samples (UFG and UFG-C), severe plastic deformed specimens with less expected dislocations inside grains revealed an advantage in corrosion resistance since a small amount of boundaries can be resulted from dislocation interactions, while well-defined extremely fine subgrains are usually observed instead of clustered dislocations in high density [3,5,11,12,14]. Moreover, it is believed that the passive film was formed at surface crystalline defects in these samples, and a higher number of nucleation sites was available to make possible a denser and more compact oxidized layer onto material surface [3,14]. This finding agrees with our results, where a predominant anatase (Figure 3) film was denser and tightly adhered onto ultrafine-grained specimens (Figure 2).

5. Conclusions

Ultrafine-grained titanium obtained by ECAP techniques has improved the corrosion resistance in comparison to its coarse-grained counterparts. Commercially pure grade 2 and 4 showed similar corrosion susceptibility. Ti-6Al-4V alloy (grade 5) showed a thin and tightly adhered native oxide layer. Surface etching revealed improvements in corrosion resistance. Ultrafine-grained titanium samples showed a more compact and adhered oxidized layer which is responsible for the higher resistance demonstrated by these samples.

Author Contributions: Dr Fernandes conceived this study, prepared manuscript, interpreted and discussed results with Dr Elias, Dr Valiev and Dr Prokofiev. Dr Elias and Dr Valiev previewed, reviewed and approved the final version. SPD samples were processed by Dr Valiev and Dr Prokofiev. Surface etching was performed by Dr Elias and Dr Fernandes. Miss Almeida and Miss Monteiro acquired polarization curves, revised its calculations and executed XRD at grazing incidence.

Funding: This research was funded by [Carlos Chagas Foundation for Research Support from the Rio de Janeiro State (FAPERJ)] grant numbers [E-26/201.759/2015, E-26/201.828/2015, E-26/010.001.262/2015], [Russian Ministry for Education and Science] contract number [14.B25.31.0017], [Saint Petersburg State University] grant number [6.37.204.2016] and [National Council of Technological and Scientific Development from Brazilian Government (CNPq)] grant number [168807/2017-3].

Acknowledgments: The authors thank Dr Chia-Hui Lu for acquisition of TEM micrographs.

Conflicts of Interest: The authors declare no conflict of interest.

References

1. Williams DF. Titanium for medical applications. In: Brunette DM, Tengvall P, Textor M, Thomsen P. (eds) 2001 *Titanium in Medicine*. Springer-Verlag: Berlin, Germany, 2001; pp. 13-24, ISBN 9783642564864.
2. Liu, H.; Xu, Q.; Zhang, X.; Wang, C.; Tang, B. Wear and corrosion behaviors of Ti6Al4V alloy biomedical materials by silver plasma immersion ion implantation process. *Thin Solid Films* **2012**, *521*, 89-93.
3. Balyanov, A.; Kutnyakova, J.; Amirkhanova, N.A.; Stolyarov, V.V.; Valiev, R.Z.; Liao, X.Z.; Zhao, Y.H.; Jiang, Y.B.; Xu, H.F.; Lowe, T.C.; Zhu, Y.T. Corrosion resistance of ultra fine-grained Ti. *Scripta Mater* **2004**, *51*, 225-229.
4. Billi, F.; Onofre, E.; Ebramzadeh, E.; Palacios, T.; Escudero, M.L.; Garcia-Alonso, M.C. Characterization of modified Ti6Al4V alloy after fretting–corrosion tests using near-field microscopy. *Surf Coat Tech* **2012**, *212*, 134-144.
5. Fernandes, D.J.; Elias, C.N.; Valiev, R.Z. Properties and Performance of Ultrafine Grained Titanium for Biomedical Applications. *Mater Res* **2015**, doi: http://dx.doi.org/10.1590/1516-1439.005615.
6. Valiev, R.Z.; Zhilyaev, A.P.; Langdon, T.G. *Bulk Nanostructured Materials: Fundamentals and Applications*, 1st ed.; John Wiley & Sons Inc: New Jersey, Canada, 2014; pp. 440-470, ISBN 1118095405.

7. Semenova, I.P.; Valiev, R.Z.; Yakushina, E.B.; Salimgareeva, G.H.; Lowe, T.C. Strength and fatigue properties enhancement in ultrafine-grained Ti produced by severe plastic deformation. *J Mater Sci* **2008**, *43*, 7354-7359.
8. Gunderov, D.V.; Polyakov, A.V.; Semenova, I.P.; Raab, G.I.; Churakova, A.A.; Gimaltdinova, E.I.; Sabirov, I.; Segurado, J.; Sitdikov, V.D.; Alexandrov, I.V.; Enikeev, N.A.; Valiev, R.Z. Evolution of microstructure, macrotexture and mechanical properties of commercially pure Ti during ECAP-conform processing and drawing. *Mater Sci Eng A* **2013**, *562*, 128–136.
9. Dyakonov, G.S.; Zemtsova, E.; Mironov, S.; Semenova, I.P.; Valiev, R.Z.; Semiatin, S.L. An EBSD investigation of ultrafine-grain titanium for biomedical applications. *Mater Sci. Eng A* **2015**, *648*, 305–310.
10. Nazarov, D.V.; Zemtsova, E.G.; Solokhin., A.Y.; Valiev, R.Z.; Smirnov, V.M. Modification of the Surface Topography and Composition of Ultrafine and Coarse Grained Titanium by Chemical Etching. *Nanomaterials* **2017** *7*, 15, doi:10.3390/nano7010015.
11. Elias, C.N.; Fernandes, D.J.; de Biasi, R.S. Comparative study of compressive and fatigue strength of dental implants made of nanocrystalline Ti Hard and microcrystalline Ti G4. *Fatigue Fract Engng Mater Struct* **2017**, *40*, 696-705.
12. Elias, C.N.; Fernandes, D.J.; Resende, C.R.S.; Roestel, J. Mechanical properties, surface morphology andstability of a modified commercially pure high strength titanium alloy for dental implants. *Dent* Mater **2015**, *31*, e1-e13.
13. Drevet, R.; Aaboubi, O.; Benhayoune, H. In vitro corrosion behavior of electrodeposited calcium phosphate coatings on Ti6Al4V substrates. *J Solid State Electrochem* **2012**, *16*, 3069-3077.
14. Kim, H.S.; Yoo, S.J.; Ahn, J.W.; Kim, D.H.; Kim, W.J. Ultrafine grained titanium sheets with high strength and high corrosion resistance. *Mater Sci Eng A* **2011**, *528*, 8479-8485.
15. Liu, X.; Chu, P.K.; Ding, C. Surface modification of titanium, titanium alloys, and related materials for biomedical applications. *Mat Sci Eng R* **2004** *47*, 49–121.
16. Takayama, I. Development of oxidation protective coating for titanium. *Nippon Steel Tech Report* **1994**, *62*, 57-63.
17. Gemelli, E.; Camargo, N.H.A. Oxidation kinetics of commercially pure titanium. *Materia* **2007**, *12*, 525-531.
18. Zhang, W.; Sadedin, D.R.; Reuter, M.A.; McCallum, J.C. The de-oxidation of partially oxidized titanium by hydrogen plasma. *Mater Forum* **2007**, *31*, 76-83.
19. Zhdanov, V.P.; Kasemo, B. Cabrera–Mott kinetics of oxidation of nm-sized metal particles. *Chem Phys Lett* **2008**, *452*, 285-288.
20. Ermoline, A.; Dreizin, E.L. Equations for the Cabrera–Mott kinetics of oxidation for spherical nanoparticles. *Chem Phys Lett* **2011**, *505*, 47-50.
21. Valiev, R.Z.; Sabirov, I.; Zhilyaev, A.P.; Langdon, T.G. Bulk nanostructured metals for innovative applications. *JOM* **2012**, *64*, 1134-1142.